High-pressure x-ray scattering and computer simulation studies of density-induced polyamorphism in silicon

Dominik Daisenberger,[1] Mark Wilson,[1] Paul F. McMillan,[1,2,*] and Raul Quesada Cabrera[1]
[1]*Department of Chemistry and Materials Chemistry Centre, Christopher Ingold Laboratories, University College London, 20 Gordon Street, London WC1H 0AJ, United Kingdom*
[2]*Royal Institution of Great Britain, Davy-Faraday Research Laboratory, 21 Albemarle Street, London W1X 4BS, United Kingdom*

Martin C. Wilding
Institute of Mathematics and Physical Sciences, University of Wales at Aberystwyth, Ceredigion, SY23 3BZ, United Kingdom

Denis Machon
Laboratoire de Physique de la Matière Condensée et Nanostructures (UMR CNRS 5586) Université Claude Bernard Lyon1, 43 Bvd du 11 Novembre 1918, F-69622 Villeurbanne, Cedex, France
(Received 6 March 2007; published 28 June 2007)

A low- to high-density pressure-driven phase transition in amorphous silicon is investigated by synchrotron x-ray diffraction in the diamond anvil cell. Complementary atomistic molecular dynamics computer simulations provide insight into the underlying structural transformations and allow us to interpret the structure factors obtained from experiment. During compression the form of the scattering function $S(Q)$ changes abruptly at 13.5 GPa, indicating significant structural rearrangement in the amorphous solid. In particular, the first peak in $S(Q)$ shifts to larger Q values. The changes are correlated with the occurrence of a low- to high-density (LDA-HDA) polyamorphic transition observed previously using Raman scattering and electrical conductivity measurements. The data are analyzed to provide real space (pair distribution function) information. The experimental data are compared with results from molecular dynamics (MD) simulations using a modified Stillinger-Weber many-body potential energy function in order to extract structural information on the densified amorphous material. We deduce that the polyamorphic transition involves an abrupt increase in the proportion of 5- and 6-coordinate Si atoms. The overall structure of the HDA polyamorph can be related to that of the LDA form by creation of highly-coordinated "defects" within the tetrahedrally-bonded LDA network. However classical and quantum MD simulations indicate that an even higher density amorphous state might exist, based on structures that resemble the densely-packed metallic polymorphs of crystalline Si.

DOI: 10.1103/PhysRevB.75.224118 PACS number(s): 64.60.−i, 61.43.Dq

I. INTRODUCTION

Silicon, in both its crystalline and amorphous forms, provides a system of fundamental technological importance. As a result, a detailed understanding of the structural and thermodynamic behavior of this system over a wide range of temperature and pressure conditions is necessary if critical applications are to be fully exploited. Studies carried out at high pressure and high temperature have revealed remarkable changes in the structure and physical properties of silicon, in its crystalline, liquid and solid amorphous states as a function of the density.

The crystalline material undergoes extensive polymorphism during compression, leading to series of metallic phases in which the Si atoms are present in octahedral, or even higher, coordination environments.[1,2] Liquid silicon at ambient pressure has metallic character and it possesses higher density than either the semiconducting (diamond) crystal or solid amorphous (a-Si) semiconducting forms of the element, that are usually prepared by chemical or physical vapor deposition methods.[3,4] Recently, a solid state chemical approach to synthesis of bulk a-Si has been described,[5] and that method was used to prepare the samples used in this study.

As a consequence of the density contrast between the crystalline polymorph and the liquid phase, diamond-structured Si-I exhibits a negative melting slope, dT_m/dP, between $P=1$ atm to 11 GPa.[6] That observation has led to analysis of the crystalline melting relations using various versions of the "two-state" model for the liquid structure.[7–9] In such models, "low-" (i.e., four-coordinate) and "high-density" structural domains are presumed to coexist in the melt, and their relative proportion changes as a function of the density. At high pressures, the high-coordinate species predominate so that the melt density is greater than that of the underlying tetrahedrally-bonded crystal and dT_m/dP is negative. As the pressure is decreased, the proportion of four-coordinate states increases so that the normal volume relations between crystal and liquid are obtained, and the dT_m/dP relation should attain a positive slope. Extension of the crystal-liquid phase relations into the negative pressure (i.e., tensile) regime using various theoretical models or computer simulations indicates that a maximum should occur in the melting curve at $P\sim-2$ to -4 GPa.[8,10–13]

At a sufficiently low temperature, that is modeled to lie below the melting line in the supercooled liquid regime, thermodynamic analyses using the two-state or two-domain models predict that the supercooled two-state liquid should encounter a critical point, followed by a line of first-order density-driven liquid-liquid phase transitions occurring between distinct low- (LDL) and high-density (HDL) super-

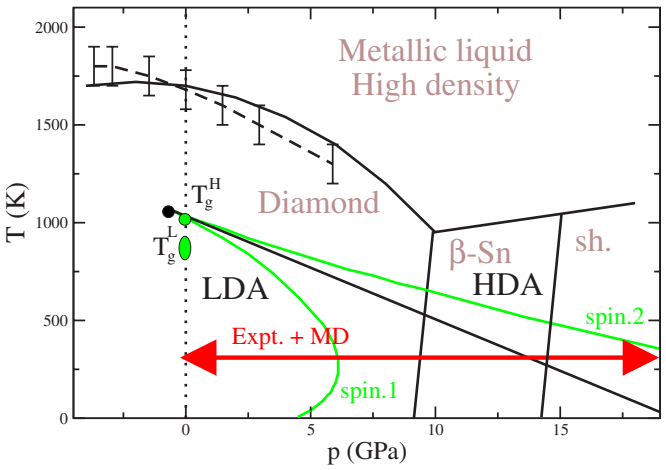

FIG. 1. (Color online) The predicted phase diagram for silicon. The crystal/liquid stability fields are obtained from a combination of molecular dynamics simulation (Ref. 13) and experiment (Refs. 2 and 47) and show the presence of both the high pressure β-Sn (Si-II) and simple hexagonal (Si-V) polymorphs within the present experimental pressure range. The metastable LDA/HDA transition line and the two spinodal lines are obtained using a two-state model as described in the text. Also shown are the respective LDL and HDL glass transition temperatures obtained from experiment (Ref. 18) and simulation. (Ref. 11) The arrow indicates the transition probed by the combination of simulation and experiment in the present work.

cooled liquid phases (Fig. 1).[7–10,14] It is difficult to directly study the LDL-HDL phase transition experimentally in the supercooled liquid, because of the extreme rapidity of crystallization occurring in the metastable high-T,P regime. Nevertheless, *in situ* high-temperature x-ray scattering experiments on liquid-Si show a change in the structure factor, $S(Q)$, and an associated drop in the coordination number from $\sim$6.5 to $\sim$5.5 during supercooling at atmospheric pressure.[15,16] However, rapid crystallization occurs before any liquid-liquid transition is observed [similar behavior is observed for l-Ge (Ref. 17)]. As the temperature is lowered, it is expected that each of the LDL and HDL phases will encounter their respective glass transformations, below which they will become nonergodic LDA and HDA amorphous solids. Although these are not true phases in internal thermodynamic equilibrium, their transformations may be considered to map on to the LDL-HDL polyamorphic liquid-liquid phase transition, assuming some similarity between the configurational energy landscapes of LDA-LDL and HDA-HDL polymorphs. Fast time-scale (ion hammering) techniques[18] predict a glass transition temperature for the LDL phase, T_g^L, at $T\sim 800-950$ K (when extrapolated to "normal" cooling rates[19]). The corresponding HDL glass transition temperature is, as yet, unknown. However, MD simulations predict such a transition at $T_g^H \sim 1027$ K.[11] The pressure dependence of both glass transition temperatures is unknown.

The two-state model of the liquid state in silicon is supported by classical and *ab initio* molecular dynamics (MD) simulations[11,20,21] and x-ray scattering experiments on Si (and Ge) as a function of the temperature at ambient pressure,[15,22,23] as well as MD simulations at high pressure and temperature.[24–26] Figure 1 shows a region of the silicon phase diagram highlighting the stable thermodynamic transitions (generated using a Stillinger-Weber potential model[27]) along with the metastable LDA and HDA fields calculated from a two-state model using values for the respective enthalpy, entropy and volume changes of $\Delta H=23.24$ kJ mol^{-1}, $\Delta S=22.0$ J mol^{-1} K^{-1} and $\Delta V=-1.2\times 10^{-6}$ m^3. MD simulations have determined the critical temperature as $T\sim 1060$ K (Ref. 11) which fixes the energy mixing parameter as $W=17.625$ kJ mol^{-1}. Both the β-Sn (Si-II) and simple hexagonal (Si-V) polymorphs have stability fields within the experimentally-accessed pressure range. The two-state model predicts a room temperature LDA to HDA pressure-driven phase transition at $p\sim 13.7$ GPa.

The first evidence for a semiconductor-metal transition in a-Si was provided by Minomura,[28] from electrical conductivity measurements carried out in a large-volume press. It was observed that at $P\sim 10$ GPa the resistance dropped by about five orders of magnitude. Upon decompression to below $P\sim 2-4$ GPa, the conductivity of the sample returned to its original value. X-ray examination of the sample following the decompression and recovery to ambient conditions showed that it was fully amorphous. It was suggested that a structural or phase transformation had occurred in the amorphous state, between semiconducting and metallic varieties of the amorphous solid element.[29] The disadvantage of these experiments was that the sample could not be examined *in situ*, and so any metastable structural or phase transformations including crystallization or reamorphization could not be observed and their possible contributions to the electrical behavior detected. In a later study of a-Si and a-Ge in a large volume apparatus using synchrotron radiation to penetrate the sample assembly and record x-ray diffraction patterns *in situ* at high pressure, it was shown that the amorphous semiconductors crystallized into their metallic β-Sn structured polymorph above $P=8-10$ GPa, and that the crystalline high-pressure phase subsequently reamorphized into the semiconducting state during decompression.[30] It was thus concluded that the resistance change observed in the earlier studies was not due to a transformation within the amorphous material, but to pressure-induced crystallization followed by reamorphization during recovery of the sample to ambient conditions. That result appeared to be confirmed by amorphous diffraction experiments in a diamond anvil cell (DAC).[31] a-Ge and a-Ge:H samples were investigated up to 10 GPa by laboratory x-ray scattering. At ambient pressure, first and second amorphous diffraction peaks (the FDP and SDP respectively) in $S(Q)$ were observed at 2.0 and 3.5 Å^{-1}. Upon pressurization, the SDP remained essentially unchanged in position, but the FDP moved to larger Q values and its width decreased.[31] Above 6.2 GPa, Bragg peaks due to crystallization of the β-Sn structured phase were present in the diffraction pattern. Some crystalline material was also present in the sample recovered to ambient conditions.

The HDA metallic form of a-Si was first identified following high-pressure amorphization experiments on porous silicon (π-Si),[10] prepared by electrolytic methods[32] and it was compressed in a DAC and studied by optical spectroscopy to investigate changes in the bandgap with pressure. Above

$P=14-16$ GPa, it was noted that the sample became black and reflective to visible light and that Raman scattering spectra indicated an amorphous structure. The pressure-induced amorphization (PIA) was confirmed by energy-dispersive synchrotron x-ray diffraction.[10] The Raman spectrum obtained at high pressure was quite different from that of the usual LDA form of silicon observed at ambient pressure, and it was concluded that HDA had been formed during PIA. During decompression, the HDA polyamorph was observed to back-transform to LDA below $P\sim 5$ GPa, with no evidence for crystallization.[10]

Recently, we conducted a high pressure study of the density-driven polyamorphic transformation between LDA and HDA-Si forms at ambient temperature using Raman spectroscopy and electrical conductivity measurements in the DAC.[12] The sample used was prepared in bulk form by a solid-state chemical metathesis method using Zintl phase NaSi as a starting material.[5] The LDA-HDA transition was observed as a dramatic change in the vibrational density of states (VDOS), as probed by Raman scattering, between $P=14-15$ GPa. The characteristic Si-Si stretching and deformation modes of the tetrahedrally-coordinated amorphous network were replaced by features concentrated in the lower frequency range, consistent with transformation to a structure with higher average coordination. This was confirmed by molecular dynamics simulations of the VDOS using a many-body Stillinger-Weber potential.[12,27] There was no evidence for crystallization in the Raman spectra obtained during compression while the appearance of the sample changed across the LDA-HDA transition. The LDA sample loaded into the DAC was a pressed powder of the amorphous semiconductor and exhibited minimal reflection of visible light during optical illumination. Above the pressure-driven transition, the HDA polyamorph appeared highly reflective, comparable with that of the metallic gasket used to contain the sample in the DAC.[12] Electrical conductivity experiments carried out in the DAC showed a large resistance drop associated with the LDA-HDA transformation, analogous to that observed in the crystalline state during the diamond-structured (Si-I) to β-Sn (Si-II) semiconductor-metal transition[1] and so we concluded that the HDA polyamorph of a-Si has metallic character. The polyamorphic transformation was found to be reversible upon release of the pressure, with considerable hysteresis as expected for a transition that corresponds to an underlying first-order density-driven liquid-liquid phase transition. During most decompression runs the observed Raman spectra exhibited no evidence for crystallization, especially if a critical region between 12–9 GPa was bypassed rapidly.[12] However, in some runs, partial recrystallization into a β-Sn structure was observed. That result is discussed further below, in the context of our present results using x-ray amorphous diffraction to study the LDA-HDA transition. During the previous study, we concluded that (a) a reversible LDA-HDA transformation in a-Si did exist; (b) the HDA polyamorph had a metallic character and it contained Si species in a higher average coordination than fourfold, in contrast to the LDA form that is semiconducting and essentially tetrahedrally coordinated; (c) the large hysteresis observed for the HDA-LDA transformation during decompression indicated its likely association with a predicted density-driven first-order liquid-liquid transition occurring in the supercooled liquid state, observed below the glass transformation range in the amorphous solid state at $T=300$ K. Such a thermodynamic phase transition has also been predicted from MD simulations[11] (Fig. 1).

In the present study, we have used synchrotron-based amorphous x-ray scattering using angle-dispersive techniques, combined with MD simulations of the amorphous structure factor and radial distribution functions, to investigate the polyamorphism in a-Si as a function of pressure.

II. EXPERIMENTAL METHODS AND DATA ANALYSIS

A. Diamond anvil cell x-ray amorphous scattering

1. Experimental details

With the development of intense highly-collimated x-ray beams available at synchrotron sources it has become possible to measure the weak x-ray scattering from noncrystalline, low Z materials at high pressure.[33,34] Energy dispersive x-ray diffraction (EDXRD) techniques have usually been employed in combination with careful spatial filtering of the scattered radiation in experiments involving large volume presses.[35,36] The technique has also been applied to study amorphous materials in the diamond anvil cell (DAC) at high pressure.[34] The EDXRD method involves passing a polychromatic "white" beam through the sample and collecting the data at several diffraction angles (2θ). The intensity must be normalized to the spectrum of the incident radiation, that is determined by the source and optics. A major challenge in such studies is to take proper account of the large background signals generated by the pressure vessel.[37] Angle dispersive (ADXRD) methods, in which a monochromatic incident x-ray beam is used, are being increasingly applied in high pressure studies of crystalline as well as amorphous materials, in the DAC as well as large volume presses. The ADXRD technique is combined with multichannel collimators (for large volume press ecperiments) and image plate or CCD camera detectors to obtain more direct and accurate intensity information.[37,38]

For high pressure amorphous x-ray scattering studies in the DAC, the main corrections to the data involve removal of the background scattering contributions from the diamond anvils.[33,39] This background scattering consists of Compton scattering and thermal diffuse scattering contributions, as well as Bragg diffraction from the diamond windows. The Bragg diffraction appears as well-defined spots in the two-dimensional 2D data sets, that can be readily masked during integration around the Laue rings to yield the amorphous diffraction intensity. Both the Compton scattering and thermal diffuse scattering contributions from diamond can be evaluated and subtracted from the data by performing a background measurement in the DAC mounted in the beam with the same orientation, but with no sample present.

Experimental factors that limit amorphous diffraction experiments in the DAC include the sample volume relative to the diameter and intensity of the collimated incident beam that is necessary to obtain a useful signal in the allocated

time; these parameters also determine the maximum pressure that can be attained in the experiment. Another consideration for amorphous diffraction studies is to obtain as large a Q range as possible for subsequent data analysis: that is determined by the opening angle of the DAC on the data collection side. Using light-element diamond seats (e.g., Be) can alleviate part of this problem. In our work we used a gas-operated membrane DAC (Ref. 40) with an opening angle of 30° (2θ=15°), with x-ray transparent Be seats for the diamond anvils to optimize the available scattering angle range. We used 2 mm diamond anvils with 650 μm culets in these experiments. The sample chamber was defined by a 300 μm hole drilled in a Re gasket. Re was chosen partly for its mechanical strength so that the gasket hole would not collapse during the experiment. The initial sample thickness was 90 μm. The DAC parameters were chosen to achieve useful amorphous scattering data from the low Z sample (a-Si) within the available beamtime at the synchrotron station, to pressures into the 20 GPa range where the polyamorphic transition is expected to occur.

No pressure transmitting medium was added into the sample chamber, to avoid having to subtract an additional signal from the measured data, and to maximize the scattered intensity from the sample. From laboratory Raman experiments carried out prior to the synchrotron run, we determined that the absence of a pressure-transmitting medium did not affect the LDA-HDA transition observed by electrical conductivity measurements or Raman scattering in the a-Si material. Likewise, we did not add a pressure calibrant such as ruby to the sample chamber, to avoid having to subtract Bragg diffraction signals from the ruby crystals from the amorphous scattering data. In laboratory experiments carried out prior to the synchrotron run, we used ruby fluorescence to calibrate the pressure achieved inside the cell relative to the gas membrane pressure, that enabled us to determine the pressure during the x-ray scattering experiments.

During amorphous diffraction studies it is important to obtain as large a Q range as possible within the obtained $S(Q)$ scattering data set, to minimize truncation errors in its Fourier transform to obtain the radial distribution function $g(r)$. For a given DAC geometry, the accessible Q range is expanded by using high energy x-rays available at third-generation synchrotron sources. In the present work data were collected at the ID-15A station of the ESRF using 52 keV x-rays, resulting in the maximum momentum transfer of Q_{max}=11 Å^{-1} (λ=0.238 431 Å) observed in these experiments (Fig. 2). The sample used here was H-free a-Si prepared by a solid-state metathesis reaction from Zintl phase NaSi. The structural state and chemical composition of that material has been described previously.[5] We reduced the beam size to 0.1×0.1 mm, exposure times varied between 1–3 min (to avoid detector saturation) and data were collected over multiple exposures to improve the counting statistics. The angle dispersive x-ray scattering data were recorded as Laue rings using a MAR3450 on-line scanning image-plate detector. 2D scattering data were transformed to integrated $I(Q)$ plots using Fit-2D software, which also implements a polarization correction.[41] Background spectra were collected using the same beam size and exposure times,

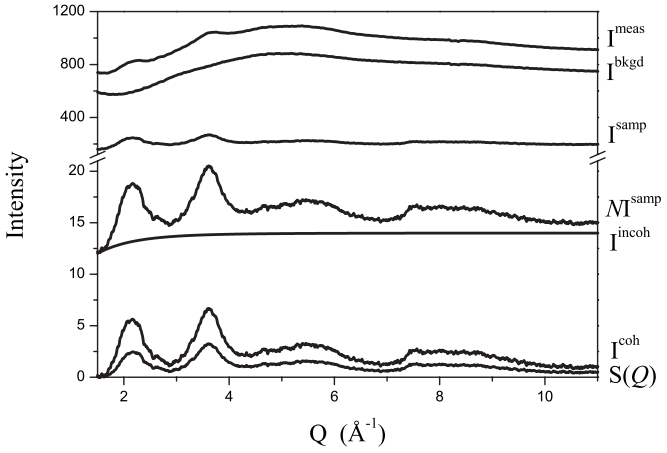

FIG. 2. The analysis of the raw x-ray diffraction data to give the final structure factor. The example shown is for the experimental x-ray data taken at the lowest pressure studied on the compression cycle. The raw x-ray scattering data (I^{meas}) obtained in the diamond anvil cell at the ID-15A station at the ESRF using 52 keV x-rays is treated as described in the text. The figure shows the background signal (I^{bkgd}) obtained from the same station under the same conditions in the absence of the sample, which is combined with I^{meas}. to give the unnormalized sample scattering (I^{samp}). The normalized sample scattering (NI^{samp}) is decomposed into the Compton scattering (I^{Incoh}) and coherent scattering (I^{coh}) contributions from which the final structure factor, $S(Q)$ is obtained.

after removal of the sample and replacing the cell in the beam path in the same orientation.

2. Data analysis

The experimental scattering data were analyzed using the following procedure. The total experimentally measured intensity, $I^{meas}(Q)$, contains various contributions from the sample and the background (Fig. 2)

$$I^{meas}(Q) = T(Q)I^{samp}(Q) + sI^{bkgd}(Q).$$

Here, $T(Q)$ and s are the DAC transmission and background scale factors; $I^{bkgd}(Q)$ is the measured empty-cell background. The scale factor is not unity due to variations in beam intensity during the course of an experiment. By introducing a normalization factor N the total scattering from the sample, $I^{samp}(Q)$, is expressed as a sum of coherent $I^{coh}(Q)$, and incoherent scattering, $I^{incoh}(Q)$

$$NI^{samp}(Q) = I^{coh}(Q) + I^{incoh}(Q).$$

The incoherent scattering contribution can be computed analytically[42] and N is found using the Krogh-Moe-Norman method[43,44]

$$N = \frac{-2\pi^2 n_0 Z^2 + \int_0^{Q_{max}} \{[f^2(Q) + I^{incoh}(Q)](Q^2)\} dQ}{\int_0^{Q_{max}} [I^{samp}(Q)] dQ}.$$

Here n_0 is the average number density, Z is the atomic number and $f(Q)$ is the atomic form factor. The structure factor is obtained by

$$S(Q) = \frac{1}{f^2(Q)}[NI^{\text{samp}}(Q) - I^{\text{incoh}}(Q)] = \frac{I^{\text{coh}}(Q)}{f^2(Q)}.$$

The real-space distribution function, $g(r)$, is the Fourier transform of $S(Q)$

$$g(r) = 1 + \frac{1}{2n_0\pi^2 r}\int_0^{Q_{\max}} Q[S(Q) - 1]\sin(rQ)dQ$$

which is exact for $Q_{\max}=\infty$. However, all experimentally determined $S(Q)$ functions have a finite $Q_{\max}$, that can lead to unphysical oscillations appearing in the real space distribution functions following the Fourier transformation procedure. In the present case, $Q_{\max}=11$ Å^{-1}; the effects of finite window size on $g(r)$ are discussed below. For normalization and subsequent $g(r)$ calculation from the experimental data the number density of a-Si at ambient conditions was used.[45] It has been shown previously that the density has only a minimal effect on the positions of the peaks in both $S(Q)$ (through the normalization procedure) and $g(r)$.[39]

In Figs. 3(a) and 3(b), we show the raw data (I^{meas}) obtained during a typical compression to $P\sim16.5$ GPa and subsequent decompression. Above ~10 GPa partial crystallization of the sample into the β-Sn (Si-II) polymorph occurs, as evidenced by the emergence of Bragg peaks. Although crystallization of phases including Si-XI (Refs. 46 and 47) and simple hexagonal Si-V (Ref. 2) phases are expected within this pressure range, the crystalline diffraction data were best indexed to Si-II (Fig. 3). The implications of such metastable crystallization are discussed below. The Raman spectrum of Si-II has previously been measured up to 16.4 GPa.[48] We also observed the appearance of Si-II in our Raman studies during certain decompression experiments, while we were investigating the LDA-HDA transition.[12] However, the crystalline signal from Bragg peaks of Si-II only makes a small contribution to the overall x-ray signal, that remains dominated by the scattering from a-Si throughout most of the pressure range. Analyzing the relative areas under the crystalline Bragg features vs. the amorphous scattering intensity yields a maximum contribution of ~30% for the highest pressure data sets. We can reconcile the observation that no Si-II signals were detected by laboratory Raman scattering carried out for the sample prior to the synchrotron run by the fact that the micro-Raman experiments probe small spatially defined regions (e.g., 5–10 μm) mainly at the sample surface, whereas the x-ray studies investigate the entire sample volume. In order to focus our attention on the (dominant) amorphous structure, the Bragg peaks of crystalline Si-II were removed from the raw data prior to further analysis (Fig. 4). It is obvious from the data presented in Fig. 3 that changes in the amorphous scattering data, especially the position of the first diffraction peak (FDP), and its intensity relative to the second amorphous scattering features (SDP), are unaffected by the occurrence of the Bragg peaks. The Bragg peaks were subtracted from the data sets by eye. The removal of the first Bragg peak near $S(Q)=2.5$ Å^{-1} (corresponding to the [200] reflection of Si-II) was straightforward. The removal of the second Bragg peak (the [220] reflection of Si-II) that occurred close to the amorphous SDP at ~3.7 Å^{-1} was more problematic. A procedure was adopted in which the Bragg peak intensity was estimated relative to the [200] feature, and then removed from the amorphous scattering data using a linear baseline function.

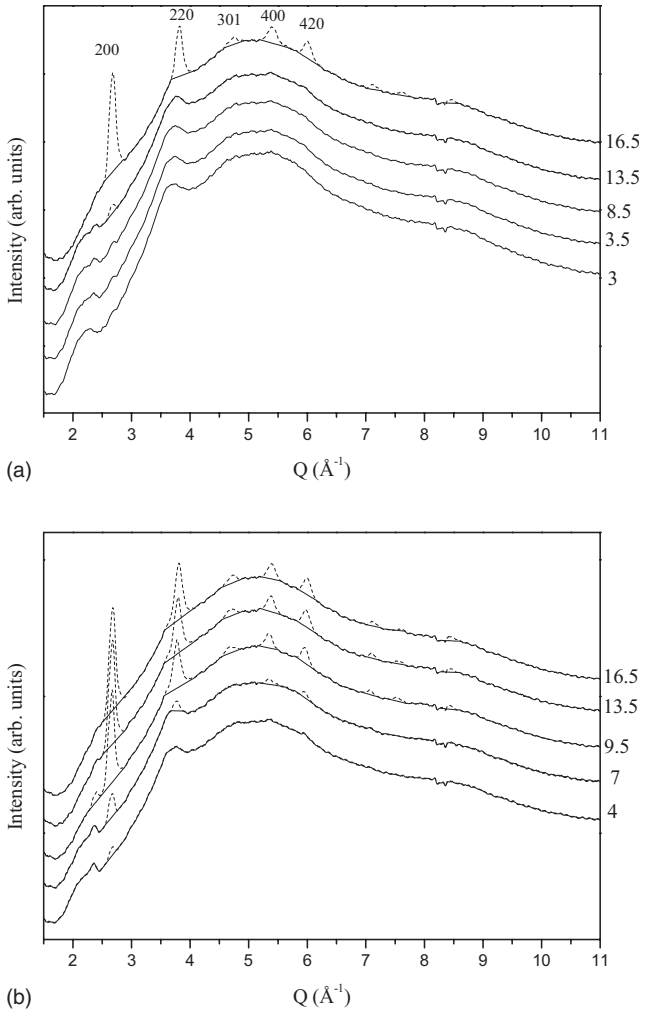

FIG. 3. The raw x-ray scattering functions, $I^{\text{meas}}(Q)$, for the (a) compression and (b) decompression cycles. The diamond anvil cell pressures (in GPa) are indicated on the right-hand side. Each successive pressure data set is shifted along the y axis for clarity. The Bragg peaks, which emerge at the highest pressure in the compression cycle are indicated by the dashed lines in the uppermost data set and are indexed as showing the presence of the β-Sn (Si-II) polymorph. The change in position of the first diffraction peak is visible in the raw data and is not affected by the presence of Bragg peaks at the highest pressure. In the decompression cycle the Bragg peaks gradually disappear as the pressure is reduced indicative of the reamorphization of the Si-II structure.

B. Molecular dynamics computer simulation

Complementary MD computer simulations were performed using a Stillinger-Weber (SW) three-body atomistic potential.[27] Constant temperature and pressure (NpT ensemble) were imposed using Nosé-Hoover thermostats and barostats.[49–51] Runs of 310 ns were performed on a system of 216 atoms at 300 K with the pressure ramped by 1 GPa ev-

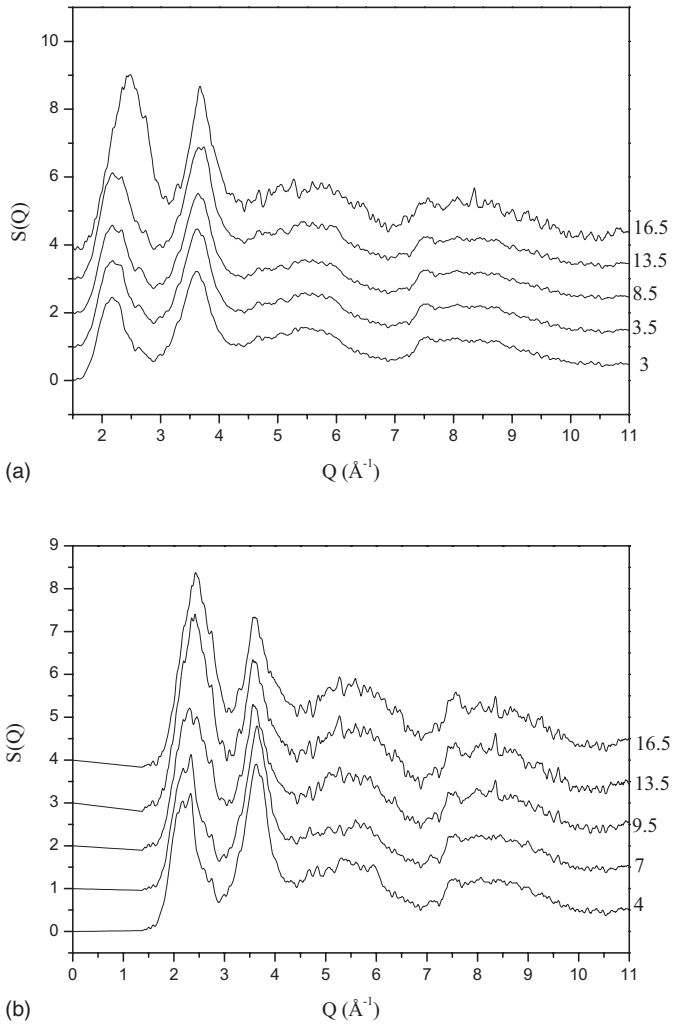

FIG. 4. Structure factors, $S(Q)$, obtained from x-ray diffraction experiments in the DAC at 300 K. Pressures (in GPa) are indicated on the right-hand side for (a) compression and (b) decompression. Successive functions are shifted by one unit along the y axis. A significant shift in the position of the first diffraction peak is observed at high pressure with a corresponding reverse shift on sample decompression.

ery 10 ns. The initial (zero pressure) amorphous configuration was obtained using a modified version of the SW potential.[52] Rapid cooling from the melt employing the original potential function results in an overcoordinated, higher density, amorphous structure, commonly referred to as "SW glass."[52] In the method developed by Luedtke and Landman,[52] weighting of the SW three-body term is increased during cooling from the melt to enhance the degree of tetrahedral order with respect to the liquid structure. This results in an amorphous structure, that is appropriately less dense than the diamond-structured crystal (i.e., Si-I), and that is dominated by tetrahedrally-coordinated sites but that contains of the order of 5.0% three-coordinate and 3.2% five-coordinate species, respectively. The experimentally determined density of annealed amorphous silicon is ~1.8% lower than that of Si-I due to the presence of such microscopic defects.[45] It is possible to obtain analogous configurations using the unmodified SW potential, with much slower cooling rates from the liquid state.[53]

The $S(Q)$ and $g(r)$ functions can be obtained directly from the MD simulation results. The $S(Q)$ is defined by $S(Q)=\langle A^*(Q)A(Q)\rangle$, where the $A(Q)=\frac{1}{\sqrt{N}}\Sigma_{i=1}^{N}e^{iQr_i}$ are the Fourier components whereas $g(r)$ is readily obtained from the distribution of pair separations. The $g(r)$ and $S(Q)$ of a-Si obtained using the modified SW potential agree very well with experimental data obtained at ambient pressure and temperature.[54,55] Other potential models, such as the environment dependent interaction potential (EDIP), have also been developed for amorphous silicon.[56,57] However, although the correct low density form of a-Si can be obtained from the melt, the EDIP-liquid is less dense than the crystal and its average coordination is too low.[58] The SW potential on the other hand gives the correct (higher) density of the liquid with respect to the crystal it and has been used successfully to investigate a wide range of system behavior, including modelling the liquid-liquid transition in supercooled liquid silicon,[11,12] and studying the relative stability and melting of clathrate phases.[13] We chose to continue our studies using the SW potential in the present work, both to interpret the $S(Q)$ data, and to place the results in the context of the metastable phase diagram (Fig. 1).

III. RESULTS

In Fig. 4(a) we show the static structure factors for a-Si obtained during experimental compression. The $S(Q)$ function is dominated by two main features; the FDP at 2.18 Å^{-1}, and the SDP at 3.63 Å^{-1}. As the pressure is increased to ~13 GPa there is a slight change in the position of the FDP (from 2.18 to 2.23 Å^{-1}) consistent with a slight densification upon pressurization. The relative intensities of the two peaks remains approximately constant on densification. Above 13.5 GPa there is a dramatic change in the structure factor. The FDP becomes more intense than the SDP and it shifts abruptly to larger Q (2.48 Å^{-1}) (Fig. 5).

During sample decompression the FDP and SDP show reversible behavior with some hysteresis [Fig. 4(b)]. Between 16.5 and 13.5 GPa the FDP is still the most intense feature and it shifts very slightly to lower Q. At 9.5 GPa the intensities of the two features are about equal and the FDP is at 2.33 Å^{-1}. After decompressing further to 4 GPa the SDP is once more the most intense feature and the FDP has shifted back to 2.18 Å^{-1}. We also note that the Bragg peaks for β-Sn crystallites (Si-II phase) that emerged during compression above 13.5 GPa, disappeared at low pressure (Fig. 3).

In Fig. 6(a) we show the series of $S(Q)$ functions for a-Si calculated from the MD simulations as a function of pressure. As the pressure is increased between 0–10 GPa the FDP shifts from 2.06–2.19 Å^{-1} and there is almost no change in the relative intensities of the first two peaks. Above 11 GPa there is a rapid reversal in the relative intensities of the FDP and SDP, and the FDP moves to 2.38 Å^{-1}. The results obtained from the MD simulations show the same changes over the same pressure range as those observed experimentally. To emphasize the similarity of the

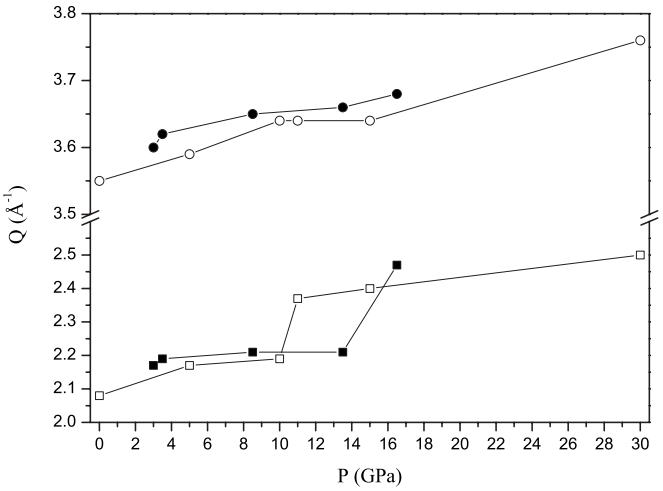

FIG. 5. The position of the first diffraction peak (FDP, squares) and second diffraction peak (SDP, circles) in the structure factors [Figs. 4 and 6(a)] as function of pressure on compression. The experimental and simulation results are shown as filled and open symbols respectively.

structure factors obtained from experiment and the MD simulation, Fig. 6(a) also shows the respective low pressure ($p \sim 3$ GPa) experimental scattering functions. At low pressure the FDP is less intense than the SDP, in agreement with previous studies at ambient pressure[54,59,60] and simulation results.

Figure 7(a) shows the radial distribution functions calculated by Fourier transformation of the experimental structure factors obtained during sample compression. The Fourier transforms of the raw data are shown as dashed lines and they exhibit significant high frequency oscillations whose wavelength is due to the truncation of the experimental reciprocal space data. The functions obtained by employing Blackman windows are shown as the solid lines. The windowing function successfully removes the high frequency oscillations; however, the resulting real space functions become broadened. However, the main features and changes in the $g(r)$ function remain unaffected. Between pressures of 3 and 13.5 GPa, the pair distribution functions show primary features at 2.36 Å and 3.83 Å associated with Si-Si bonding and next-nearest neighbor Si…Si interactions, indicative of the local tetrahedral coordination geometry. At high pressure (16.5 GPa), the second peak shifts to a shorter separation of ~3.40 Å whereas the first peak shifts to slightly longer separation. This indicates the formation of high coordinate Si species. The reverse behavior is observed during decompression [Fig. 7(b)]. The real space data displays the same hysteresis as the $S(Q)$ data so that there is little change in the peak positions between 16.5 and 9.5 GPa. As the pressure is lowered below 9.5 GPa the first peak moves back to shorter separation and the second peak shifts to 3.72 Å.

Figure 6(b) shows the analogous pair distribution functions obtained directly from the MD simulations. The ability to generate these functions from *a priori* knowledge of the atom positions means that the MD data do not suffer from the truncation effects observed for the experimental data. These functions exhibit analogous changes to the experimental compression data sets, and (in turn validating the reliability of our experimental analysis). At low pressure the $g(r)$ functions display the same two main peaks, along with a weak shoulder on the short-separation side of the second peak (~3.30 Å). As the pressure is increased, the nearest-neighbor peaks initially shifts to shorter distances and the shoulder on the second peak increases slightly in intensity. At high pressures this shoulder becomes the main feature of the second peak with a corresponding shift of the first peak in $g(r)$ to longer separations.

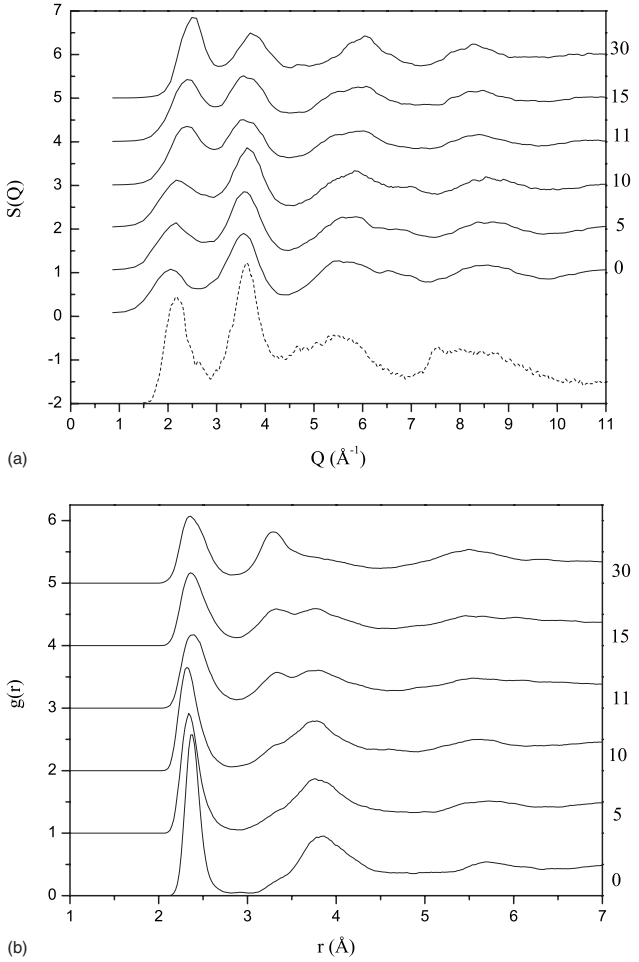

FIG. 6. (a) Structure factors and, (b) pair distribution functions, obtained from simulation as a function of pressure. The simulation cell pressures are indicated, in GPa, on the right-hand side. In both cases successive functions are shifted by one unit along the y axis for clarity. In (a) the structure factor obtained from DAC compression experiment at 3 GPa is shown as a dashed line, shifted down by two units on the y axis, showing the similarity with the structure factors obtained from MD simulation.

Making a direct link between the experimental data and the MD simulation results means that the simulations can be used to investigate other properties of the densified amorphous system. In Fig. 8, we show the p-V curves obtained from the MD simulations. There is a dramatic change in system volume at around 10.5 GPa, that corresponds to the LDA to HDA polyamorphic transformation. It is of interest that the amorphous system produced using the SW potential in the absence of the enhanced three-body term shows no

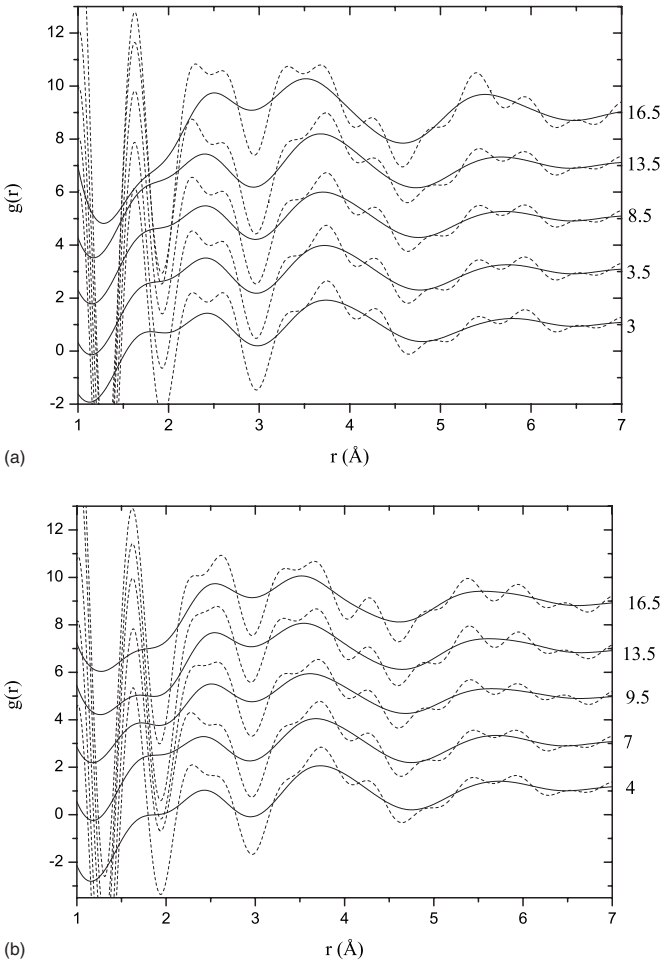

FIG. 7. Pair distribution functions, $g(r)$, obtained from the x-ray diffraction experiments by Fourier transformation of the structure factors shown in Fig. 4 for (a) compression, (b) decompression. Pressures, in GPa, are indicated on the right-hand side and successive curves are shifted by two units along the y axis. The dashed and solid lines show the result of the Fourier transforms in the absence of and with a windowing function. The windowing function successfully removes the high frequency oscillations at the expense of broadening the real space peaks.

such pressure-driven amorphous-amorphous transformation within this pressure range. Previous studies of liquid silicon in the highly supercooled regime predict that an entropy-, density-driven first-order phase transition should occur in the highly supercooled regime. The critical point is predicted to occur at slightly negative pressure, $P \sim -1$ GPa at $T \sim 1100$ K. Extrapolation to $T=300$ K using two-state models, ignoring the presence of a glass transition for either phase, leads to a prediction of $P \sim 13.5$ GPa for the LDA-HDA phase transformation. This is in good agreement with our experimental and MD simulation results. At low pressure a-Si is of lower density than the diamond-structured crystal and it has a smaller bulk modulus (Table I). The supercooled SW liquid is, as expected, more dense than the diamond crystal at the same P and T. At the transition pressure the simulated system volume changes from 18.30 Å^3 atom^{-1} to 17.38 Å^3 atom^{-1} with a corresponding

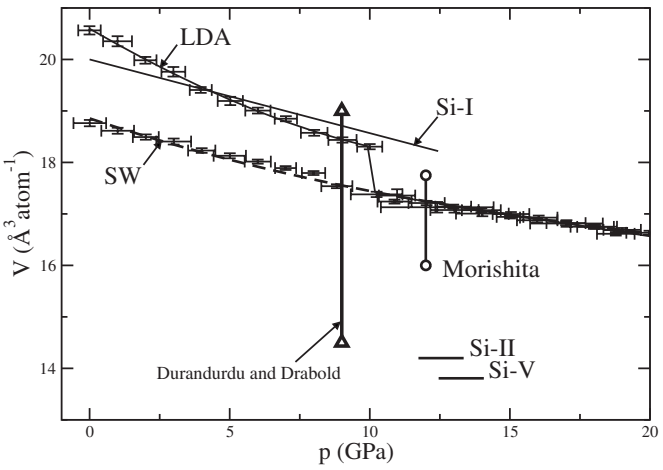

FIG. 8. Pressure-volume relations obtained from the molecular dynamics simulations. The curve marked LDA is the p-V behavior for the system obtained from the modified Stillinger-Weber potential, as described in the text, and shows a clear pressure-driven transition at 11 GPa. The curve marked SW in the p-V function was obtained using the unmodified SW potential. The vertical lines indicated by △ and ○ represent the volume changes observed by Durandurdu *et al.* (Refs. 24 and 25) and Morishita (Ref. 26) respectively. The solid line labelled Si-I shows the p-V behavior of the ideal simulated diamond crystal. The lines marked Si-II and Si-V indicate the volumes of these two polymorphs at their experimental transition pressures.

rise in the mean nearest-neighbor atom coordination number from 4.0 to 4.6.

IV. DISCUSSION

We begin by considering the pressure-volume relations (Fig. 8) established for compression of amorphous Si with respect to previous simulation studies using *ab initio* theoretical methods. Our figure indicates the volume changes observed in this study, compared with the values obtained by Morishita[26] and Durandurdu and Drabold.[24,25] Morishita observed a slightly larger volume change for the LDA-HDA polyamorphic transition than that obtained in the present work, along with a corresponding change in average coordination number from 4 to 5.1; however, the results are comparable with those obtained using the SW potential. However, Durandurdu and Drabold observed a much larger volume change occurring at 16.25 GPa, that was associated

TABLE I. Values for the volume at zero pressure, V_0, and the bulk modulus, K_0. The values for Si-I are from Hu *et al.*, (Ref. 2). while those for LDA- and HDA-Si are from our MD simulations, fitted to the second order Birch-Murnaghan EOS by using EosFit. (Ref. 69).

Table I	V_0 (Å^3 atom^{-1})	K_0 (GPa)
Si-I	20.06	98
LDA-Si	20.56	66.5
HDA-Si	18.10	181.0

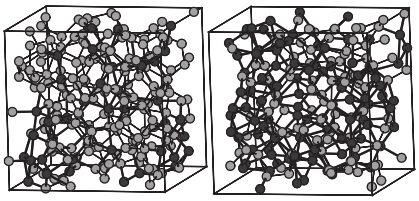

FIG. 9. Moelcular graphics "snapshots" of typical LDA (left) and HDA (right) configurations. Four and five-coordinate Si atoms are shown as the light and dark shaded circles respectively, highlighting the greater number of these five-coordinate "defect" sits in the HDA configuration.

with a change in average coordination number from 4 to ~9. The significance of that result is discussed below.

The structure of the LDA form of a-Si sample at low pressure is based on an essentially ideal tetrahedrally-coordinated network, containing very few over- or under-coordinated defects. The HDA structure described here, and also that observed by Morishita, can be understood in terms of highly-coordinated defects generated within the LDA tetrahedral network. The mean atom coordination number is increased to above four by the presence of five- or six-coordinated atoms that occupy defect sites between the tetrahedra. Figure 9 shows molecular graphics "snapshots" of an LDA and HDA configuration with the Si sites coloured according to coordination environment. The HDA phase contains a significantly higher fraction of five-coordinate "defect" sites when compared to the LDA. The concentration of these defects is, therefore, directly related to both the mean coordination number and the volume collapse observed at the transition pressure. In this picture, the differences in volume change and average coordination observed between the SW result and those obtained by Morishita reflect a slightly smaller defect concentration within the LDA structure.

Such a defect picture of the amorphous structure is supported by both x-ray diffraction and MD studies on the supercooled liquid at high temperature which show changes in the relative FDP and SDP intensities in $S(Q)$ analogous to those seen here as a function of pressure. These intensity changes correspond to a decrease in defect concentration as the liquid is cooled to ~1460 K, just above the predicted liquid-liquid transition.[15] Supercooled liquid germanium also displays such a decrease in the average coordination number and a corresponding increase in the relative amount of tetrahedral bonding.[17,61] High pressure, room temperature XAS experiments on a-Ge show a partially reversible transition to a HDA form, with an associated increase in average coordination number to 4.5.[62]

The larger volume change and significantly higher average coordination number observed in the *ab initio* simulations of Durandurdu and Drabold for both a-Si and a-Ge, might be indicative of the emergence of a "very high density amorphous" (VHDA) state. Such behavior would be analogous to that observed for amorphous H_2O, for which the structural and thermodynamic implications of the relationships between LDA-HDA-VHDA forms are currenty under discussion.[63–66] In the case of a-H_2O, a model based on coordination defects within a tetrahedral network structure has been proposed to describe the HDA polyamorph with respect to LDA, and a higher-density structure is projected for VHDA.[66]

There is significant evidence both from simulation and experimental studies that the LDA/HDA transformation maps on to a genuinely first order phase transition in the supercooled liquid state. However, it is not clear that the same would hold true for the HDA/VHDA transformation. One possibility is that there is such a first order HDA/VHDA phase transition with an associated phase boundary and an additional critical point in the system. One alternative possibility is that the transition from an HDA-like to a VHDA-like configuration is continuous and is therefore associated with a gradual increase in the number of filled defect sites as the pressure is increased. Another possibility is that there exists an series of VHDA-like phases, each characterized by a different concentration of defect sites, perhaps separated from each other by a series of phase boundaries with associated critical points.

Considering the present work in association with previous theoretical studies, one possibility is that the different simulation approaches are accessing alternative HDA vs VHDA-like states. Such differences could be determined by quite subtle aspects of the underlying simulation methodologies. For example, factors including system size and, in particular, the simulated compression rates (and, indeed, the precise details of the manner in which the pressure is applied) might be expected to be significant. These possibilities must be tested in future work by systematically varying the simulation conditions.

Our data for a-Si do not yet allow us to test the VHDA hypothesis experimentally. However, the density-driven polyamorphism can be understood by reference to analogous crystal phase transitions.[2] Figure 8 highlights the densities of the high pressure β-Sn (Si-II) and simple hexagonal (Si-V) structured phases, which contain six- and eight-coordinated atoms, respectively. The crystal densities are typical of those observed in the amorphous state from the *ab initio* simulations and, as a result, we might expect the local coordination environments associated with the VHDA phase to resemble the local (high) coordination environments displayed by these high pressure crystals.

VHDA forms have already been proposed for both amorphous silicon and germanium based on the application of high pressure to the respective liquids.[64] Funamori and Tsuji[36] noted a change in the liquid phase structure of silicon between 8 and 14 GPa to give a system whose local coordination environment was suggested to be similar to that of the simple hexagonal crystal. Similarly, Koga *et al.* demonstrated[67] how application of high pressure to liquid germanium resulted in an increase in the average coordination number to ~7.

Apart from the results for a-Si, the experimental $S(Q)$ data presented here also show the crystalline phase Si-II forming outside its normal stability field, i.e., in a highly metastable regime, followed by reamorphization during decompression to ambient pressure. From high pressure x-ray diffraction experiments, Si-II is normally observed to form from Si-I in a pressure range between 10.3 to 14 GPa,[47] whereas other crystalline polymorphs (Si-XI, Si-V) are ob-

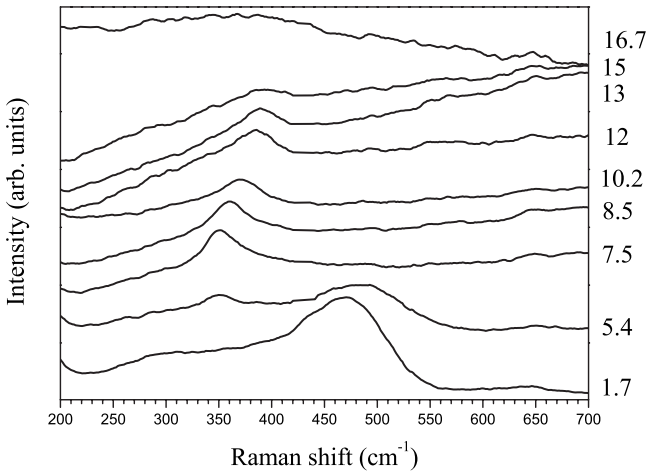

FIG. 10. Raman spectra obtained during sample decompression. The sample pressures in GPa as indicated on the right of the figure. As the pressure is lowered from 16.7 to 15 GPa, HDA-Si transforms into Si-II. Shown here is the TO mode of Si-II as the LO mode is at too low wave number to be observed in a back scattering geometry. At 5.4 GPa LDA-Si emerges and only a small amount of Si-II is still present. At 1.7 GPa the spectrum is that of LDA-Si.

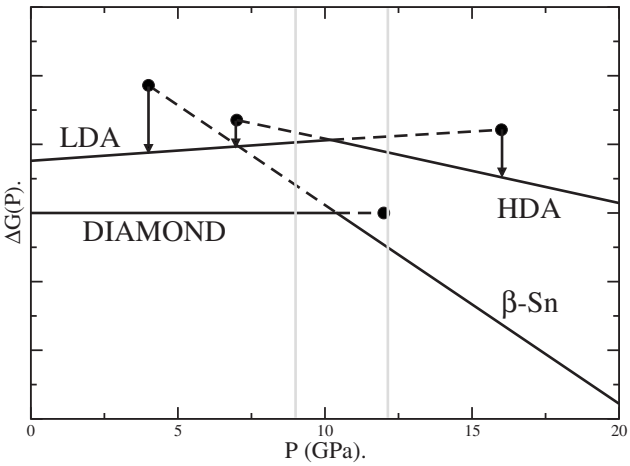

FIG. 11. A schematic $G(P)$ diagram to highlight the phase transformations observed in the present work. The free energies are shown as differences with respect to that of the diamond structure (the zero pressure ground state) in order to emphasize the observed transformations. The dashed lines show the metastable extensions accessible from experiment and the filled symbols highlight the spinodals encountered in the present work. The light vertical lines highlight the pressure range over which both the crystalline and amorphous pressure-driven phase transitions are expected to occur.

served to crystallize above these pressures.[46] Similarly, during decompression, Si-II is usually observed to persist down to 6.2 GPa. Further decompression results in metastable transformation to two further crystalline polymorphs (Si-XII, Si-III).[68] In the data presented here, on compression Si-II forms at above $P \sim 8.5$ GPa and persists to at least 16.5 GPa. On decompression, the presence of Si-II is recorded down to 4 GPa, at which point it reamorphizes into LDA-Si. During our previous Raman spectroscopic investigations of the LDA-HDA transformation and its reversal during decompression, we also observed similar metastable formation and reamorphization of Si-II during the decompression part of the cycle, when the sample was decompressed slowly within the 12–9 GPa range.[12] Those data showed the emergence of Si-II at $P \sim 15$ GPa, and subsequent reamorphization below 7.5 GPa (Fig. 10). Previously, the Raman spectrum of Si-II has been recorded up to 16.4 GPa.[48] Other compression experiments on LDA-Si have also shown the formation and persistence of Si-II at high pressure, outside its normal phase field, and that the crystals subsequently reamorphized during decompression.[28,30] At low temperature, Si-II formed from compression of Si-I has been shown to transform to LDA-Si during decompression.[6]

Figure 11 shows a schematic Gibbs free energy $G(P)$ diagram for metastable crystalline and amorphous polymorphs of silicon that can summarize these observations. The free energies are displayed as differences relative to the zero pressure ground state (the diamond structure) in order to emphasize the observed phase changes. Because $G=\text{H-TS}=U+PV\text{-TS}$, the slope is approximately equal to the molar volume (V) at constant T. As the pressure is increased a-Si encounters its LDA-HDA transition at ~ 10 GPa or, because this is a first order transformation, it can become superpressed towards the spinodal line that is predicted to occur at $P \sim 16$ GPa at ambient T (Fig. 1) at which point the HDA phase is formed. The amorphous polymorphs are metastable with respect to Si-II at all pressures above ~ 7 GPa, and, as a result, it is expected that the high-pressure crystalline phase could nucleate at any pressure within this range. On decompression of HDA the system again encounters the thermodynamic transition pressure at $P \sim 10$ GPa and is metastable to a pressure of ~ 7 GPa, at which point the system transforms back to the LDA. Likewise, the Si-II crystallites become metastable with respect to the diamond structure at $P \sim 10$ GPa and metastable with respect to the LDA phase at $P \sim 7$ GPa. At $P \sim 4$ GPa the Si-II encounters the spinodal and the system fully amorphizes to the LDA.

V. CONCLUSION

We conducted an *in situ* DAC study of the amorphous x-ray scattering in a-Si at high pressure and room temperature. The data combined with MD simulation results supported the evidence for a density-driven polyamorphic transformation occurring at $P > 10$ GPa at $T = 300$ K, in agreement with previous Raman scattering and electrical conductivity results. Analysis of the MD simulation configurations indicates that the LDA-HDA transformation may be associated with formation of defect structures within the tetrahedrally-coordinated LDA polyamorph, in which highly coordinated atoms occupy interstitial sites in the amorphous network. It is possible that even higher density amorphous states ("VHDA") exist, in which all the atoms occupy higher coordination sites.

ACKNOWLEDGMENTS

We acknowledge the ESRF for provision of synchrotron radiation facilities and V. Honkimäki and T. Buslaps for assistance in using beam line ID-15A.

*Author to whom correspondence should be addressed. Electronic address: p.f.mcmillan@ucl.ac.uk

[1] J. C. Jamieson, Science **139**, 762 (1963).
[2] J. Z. Hu, L. D. Merkle, C. S. Menoni, and I. L. Spain, Phys. Rev. B **34**, 4679 (1986).
[3] S. Roorda, K. Laaziri, and S. C. Gujrathi, Nucl. Instrum. Methods Phys. Res. B **148**, 360 (1999).
[4] W. F. v. d. Weg, A. J. M. Berntsen, F. W. Saris, and A. Polman, Mater. Chem. Phys. **46**, 140 (1996).
[5] P. F. McMillan, J. Gryko, C. Bull, R. Arledge, A. J. Kenyon, and B. A. Cressey, J. Solid State Chem. **178**, 937 (2005).
[6] V. V. Brazhkin, A. G. Lyapin, S. V. Popova, and R. N. Voloshin, Phys. Rev. B **51**, 7549 (1995).
[7] E. Rapoport, J. Chem. Phys. **46**, 2891 (1967).
[8] E. G. Ponyatovsky and O. I. Barkalov, Mater. Sci. Rep. **8**, 147 (1992).
[9] C. T. Moynihan and C. A. Angell, J. Non-Cryst. Solids **274**, 1 (2000).
[10] S. K. Deb, M. Wilding, M. Somayazulu, and P. F. McMillan, Nature (London) **414**, 528 (2001).
[11] S. Sastry and C. A. Angell, Nat. Mater. **2**, 739 (2003).
[12] P. F. McMillan, M. Wilson, D. Daisenberger, and D. Machon, Nat. Mater. **4**, 680 (2005).
[13] M. Wilson and P. F. McMillan, Phys. Rev. Lett. **90**, 135703 (2003).
[14] L. I. Aptekar, Sov. Phys. Dokl. **24**, 993 (1979).
[15] N. Jakse, L. Hennet, D. L. Price, S. Krishnan, T. Key, E. Artacho, B. Glorieux, A. Pasturel, and M. Saboungi, Appl. Phys. Lett. **83**, 4734 (2003).
[16] S. Ansell, S. Krishnan, J. J. Felten, and D. L. Price, J. Phys.: Condens. Matter **10**, L73 (1998).
[17] A. Filipponi and A. DiCicco, Phys. Rev. B **51**, 12322 (1995).
[18] A. Hedler, S. L. Klaumünzer, and W. Wesch, Nat. Mater. **3**, 804 (2004).
[19] P. F. McMillan, Nat. Mater. **3**, 755 (2004).
[20] C. R. Miranda and A. Antonelli, J. Chem. Phys. **120**, 11672 (2004).
[21] P. Keblinski, M. Z. Bazant, R. K. Dash, and M. M. Treacy, Phys. Rev. B **66**, 064104 (2002).
[22] M. Davidović, M. Stojić, and D. J. Jović, J. Phys. C **16**, 2053 (1983).
[23] P. S. Salmon, J. Phys. F: Met. Phys. **18**, 2345 (1988).
[24] M. Durandurdu and D. A. Drabold, Phys. Rev. B **64**, 014101 (2001).
[25] M. Durandurdu and D. A. Drabold, Phys. Rev. B **67**, 212101 (2003).
[26] T. Morishita, Phys. Rev. Lett. **93**, 055503 (2004).
[27] F. H. Stillinger and T. A. Weber, Phys. Rev. B **31**, 5262 (1985).
[28] S. Minomura, *High Pressure and Low-Temperature Physics* (Plenum, New York, 1978).
[29] O. Shimomura, S. Minomura, N. Sakai, K. Asaumi, K. Tamura, J. Fukushima, and H. Endo, Philos. Mag. **29**, 547 (1974).
[30] M. Imai, T. Mitamura, K. Yaoita, and K. Tsuji, High Press. Res. **15**, 167 (1996).
[31] K. Tanaka, Phys. Rev. B **43**, 4302 (1991).
[32] Y. H. Xie *et al.*, Phys. Rev. B **49**, 5386 (1994).
[33] J. H. Eggert, G. Weck, P. Loubeyre, and M. Mezouar, Phys. Rev. B **65**, 174105 (2002).
[34] C. Meade, R. J. Hemley, and H. K. Mao, Phys. Rev. Lett. **69**, 1387 (1992).
[35] Y. Katayama, T. Mizutani, W. Utsumi, O. Shimomura, M. Yamakata, and K. Funakoshi, Nature (London) **403**, 170 (2000).
[36] N. Funamori and K. Tsuji, Phys. Rev. Lett. **88**, 255508 (2002).
[37] W. A. Crichton, M. Mezouar, T. Grande, S. Stolen, and A. Grzechnik, Nature (London) **414**, 622 (2001).
[38] K. Yaoita, Y. Katayama, K. Tsuji, T. Kikegawa, and O. Shimomura, Rev. Sci. Instrum. **68**, 2106 (1997).
[39] G. Shen, V. Prakapenka, M. L. Rivers, and S. R. Sutton, Rev. Sci. Instrum. **74**, 3021 (2003).
[40] Diacell-Bragg-(G)*, EasyLab, formerly DIACELL.
[41] A. Hammersley, O. Svensson, M. Hanfland, A. Fitch, and D. Häusermann, High Press. Res. **14**, 235 (1996).
[42] V. H. Smith, A. J. Thakkar, and D. C. Chapman, Acta Crystallogr. **A31**, 391 (1975).
[43] J. Krogh-Moe, Acta Crystallogr. **9**, 951 (1956).
[44] N. Norman, Acta Crystallogr. **10**, 370 (1957).
[45] J. S. Custer, M. O. Thompson, D. C. Jacobson, J. M. Poate, S. Roorda, W. C. Sinke, and F. Spaepen, Appl. Phys. Lett. **64**, 437 (1994).
[46] M. I. McMahon, R. J. Nelmes, N. G. Wright, and D. R. Allan, Phys. Rev. B **50**, 739 (1994).
[47] G. A. Voronin, C. Pantea, T. W. Zerda, L. Wang, and Y. Zhao, Phys. Rev. B **68**, 020102(R) (2003).
[48] H. Olijnyk, Phys. Rev. Lett. **68**, 2232 (1992).
[49] S. Nosé, Mol. Phys. **52**, 255 (1984).
[50] S. Nosé, J. Chem. Phys. **81**, 511 (1984).
[51] G. J. Martyna, D. J. Tobias, and M. L. Klein, J. Chem. Phys. **101**, 4177 (1992).
[52] W. D. Luedtke and U. Landman, Phys. Rev. B **37**, 4656 (1988).
[53] W. D. Luedtke and U. Landman, Phys. Rev. B **40**, 1164 (1989).
[54] K. Laaziri, S. Kycia, S. Roorda, M. Chicoine, J. L. Robertson, J. Wang, and S. C. Moss, Phys. Rev. Lett. **82**, 3460 (1999).
[55] S. Kugler, L. Pusztai, L. Rosta, P. Chieux, and R. Bellissent, Phys. Rev. B **48**, 7685 (1993).
[56] R. Biswas and D. R. Hamann, Phys. Rev. Lett. **55**, 2001 (1985).
[57] R. Biswas, G. S. Grest, and C. M. Soukoulis, Phys. Rev. B **36**, 7437 (1987).
[58] J. F. Justo, M. Z. Bazant, E. Kaxiras, V. V. Bulatov, and S. Yip, Phys. Rev. B **58**, 2539 (1998).
[59] J. Fortner and J. S. Lannin, Phys. Rev. B **39**, 5527 (1989).
[60] S. Kugler, G. Molnár, G. Petö, E. Zsoldos, L. Rosta, A. Menelle, and R. Bellissent, Phys. Rev. B **40**, 8030 (1989).
[61] G. Kresse and J. Hafner, Phys. Rev. B **49**, 14251 (1994).
[62] E. Principi, A. DiCicco, F. Decremps, A. Polian, S. DePanfilis, and A. Filipponi, Phys. Rev. B **69**, 201201(R) (2004).
[63] R. J. Nelmes, J. S. Loveday, T. Strässle, C. L. Bull, M. Guthrie, G. Hamel, and S. Klotz, Nat. Phys. **2**, 414 (2006).
[64] C. J. Benmore, R. T. Hart, Q. Mei, D. L. Price, J. Yarger, C. A. Tulk, and D. D. Klug, Phys. Rev. B **72**, 132201 (2005).
[65] T. Loerting, W. Schustereder, K. Winkel, C. G. Salzmann, I. Kohl, and E. Mayer, Phys. Rev. Lett. **96**, 025702 (2006).
[66] T. Loerting and N. Giovambattista, J. Phys.: Condens. Matter **18**, R919 (2006).
[67] J. Koga, H. Okumura, K. Nishio, T. Yamaguchi, and F. Yonezawa, Phys. Rev. B **66**, 064211 (2002).
[68] R. O. Piltz, J. R. Maclean, S. J. Clark, G. J. Ackland, P. D. Hatton, and J. Crain, Phys. Rev. B **52**, 4072 (1995).
[69] R. J. Angel, *Equations of state*, in *High-pressure, high temperature crystal chemistry*, edited by R. M. Hazen and R. T. Downs, Rev. Mineral. Geochem. 41, (2001).